PANDA
Forward Spectrometer Calorimeter
-Shashlyk calorimeter

Chunxiu Liu

2018-12-17

RE-TDR-2015-002

Technical Design Report for the $\overline{\mathsf{P}}$ANDA Forward Spectrometer Calorimeter

(AntiProton ANnihilations at DArmstadt)

$\overline{\mathsf{P}}$ANDA Collaboration

March 27, 2017

Forward Spectrometer Calorimeter

- Introduction
- Geometry structure of the shashlik calorimeter
- FSC Geometry in the current PandaRoot version
- Calibrations
- Simulation results from TDR of FSC
- What do we need to do ?

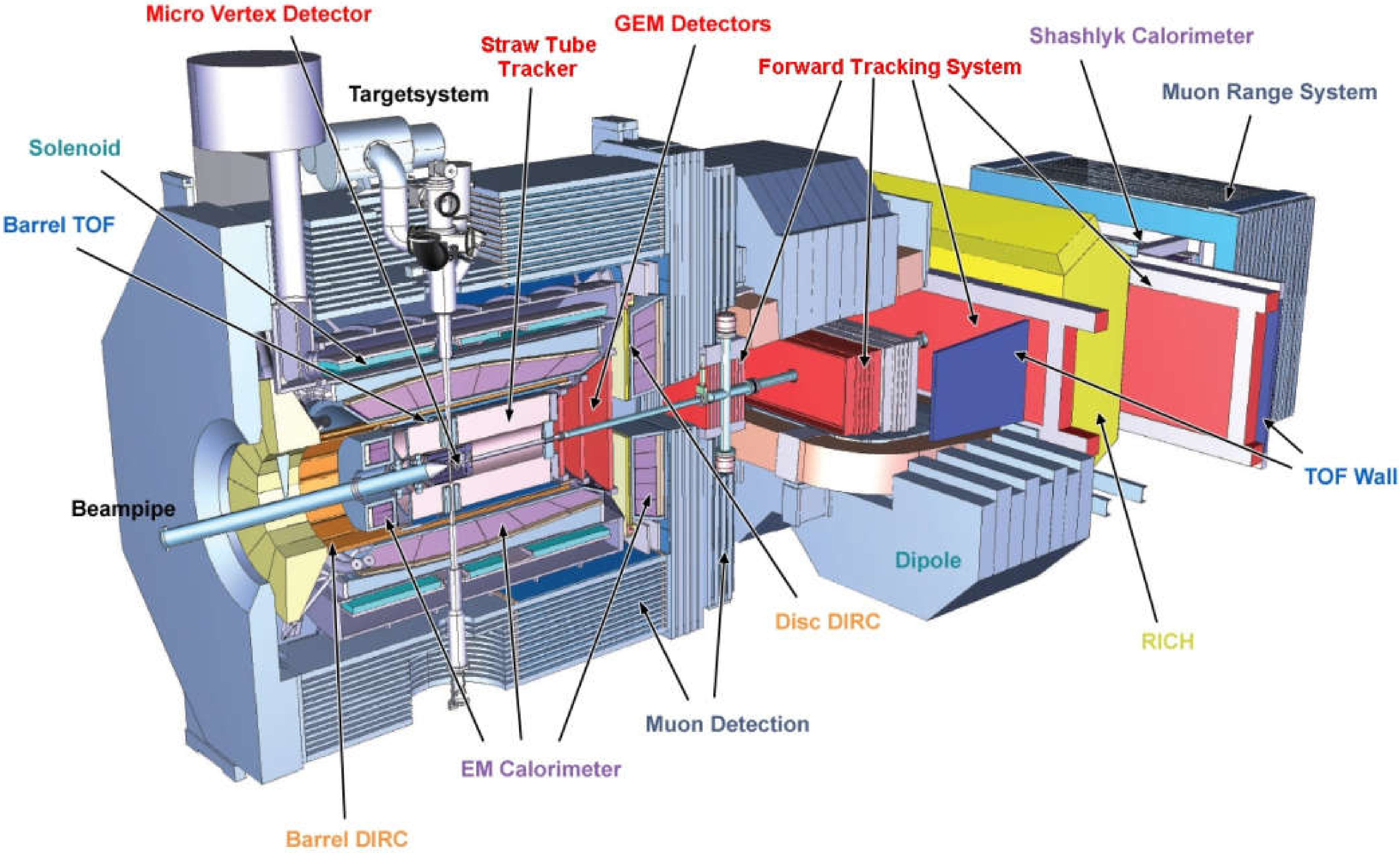

Micro Vertex Detector
GEM Detectors
Straw Tube
Tracker
Shashlyk Calorimeter
Forward Tracking System
Targetsystem
Muon Range System
Solenoid
Barrel TOF
TOF Wall
Beampipe
Dipole
Disc DIRC
RICH
Muon Detection
EM Calorimeter
Barrel DIRC

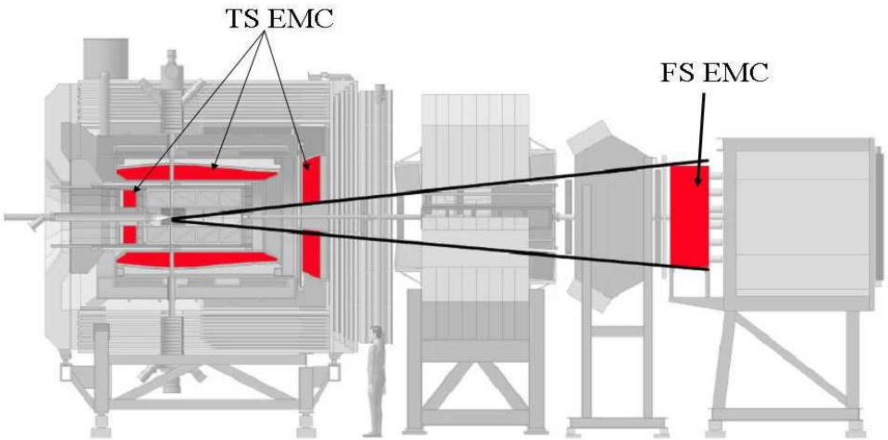

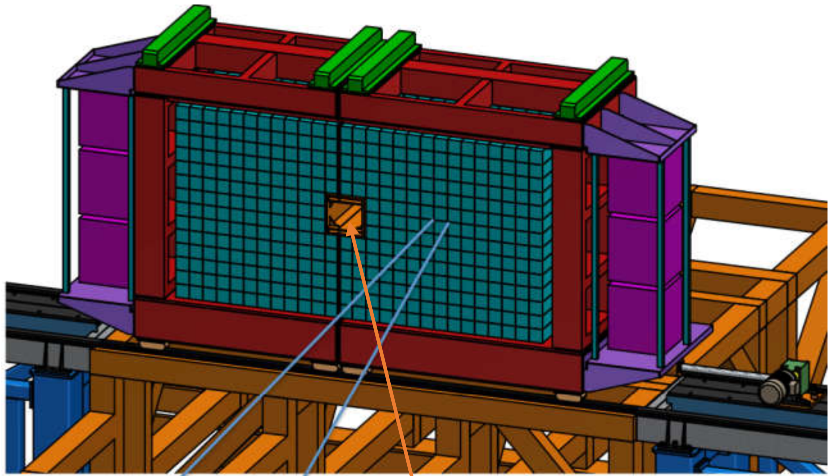

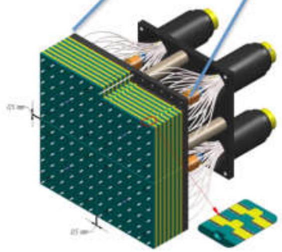

One module

The hole is 3x3 modules

- the shashlyk wall is at a distance of 7.8 m from IP
- 5° in vertical and 10° in horizontal direction.
- two parts : the left and right side of the beam pipe
- a bit asymmetric (12 modules on the left and 15 modules on the right), due to the influence of the magnetic dipole field on charged particles

Table 3.1: Requirements for the $\overline{\mathrm{P}}$ANDA FSC. Rates and doses are based on a luminosity of L = $2{\cdot}10^{32}$ $cm^{-1}s^{-1}$.

Common properties	Required performance value
energy resolution σ_E/E	$\approx$ (2-3)% / $\sqrt{E/GeV}$ $\oplus$ 1%
energy threshold (photons) E_{thres}	10 MeV (20 MeV tolerable)
energy threshold (single cell) E_1	3 MeV
noise (energy equiv.) σ_{Enoise}	1 MeV
angular coverage	0°- 5°
energy range from E_{thres} to	15 GeV
spatial resolution	3.5 mm
load per cell	$\approx$ 1 MHz
radiation hardness (maximum integrated dose)	10 kGy

At KOPIO With 11cm*11cm,One module

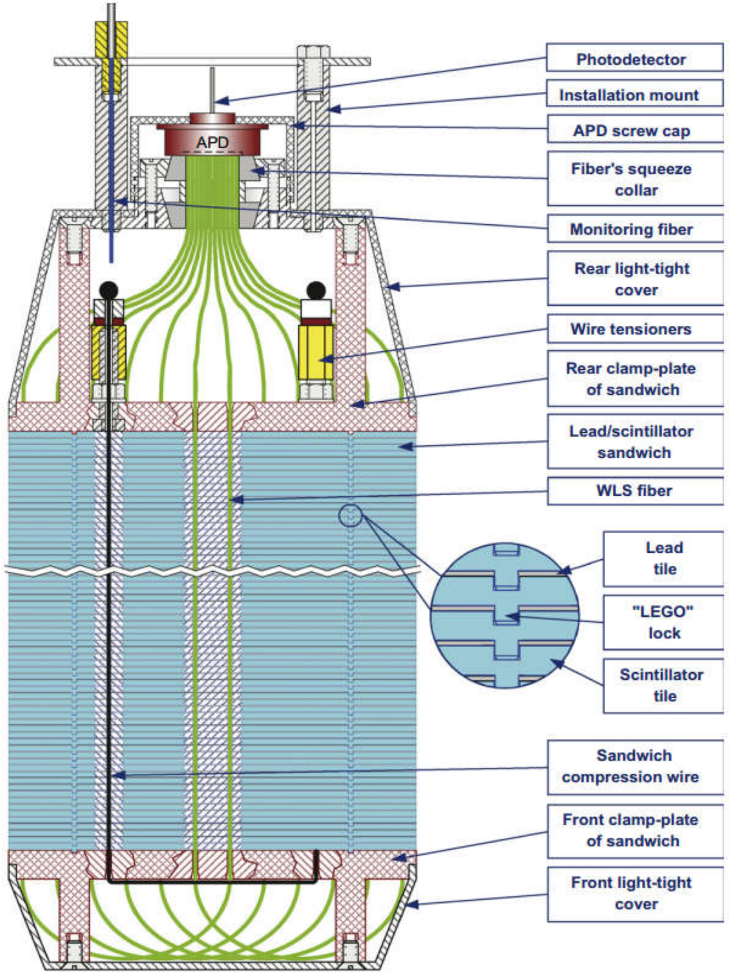

Fig. 1. The Shashlyk module design.

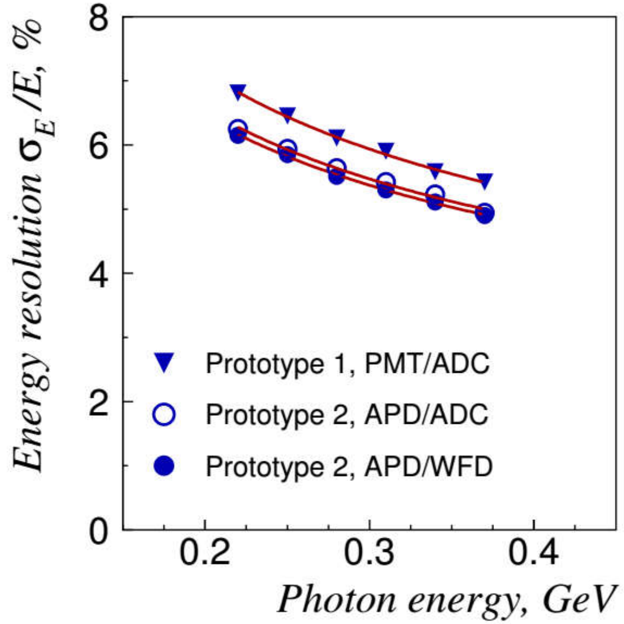

Figure 8.1: Energy resolution for KOPIO prototype calorimeters [2].

$$\frac{\sigma_{\mathrm{E}}}{\mathrm{E}}[\%] = \frac{(2.74 \pm 0.05)}{\sqrt{\mathrm{E/GeV}}} \oplus (1.96 \pm 0.1)$$

Module

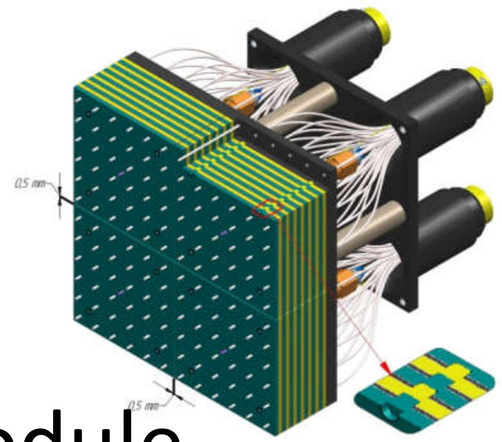

Figure 4.5: 3D view of the stack of scintillator tiles locked by LEGO-type pins and holes.

Lateral dimension of a module	$(11 \times 11)cm^2$
Lateral dimension of a cell	$(5.5 \times 5.5)cm^2$
Lead plate thickness	0.275mm
Scintillator tile thickness	1.5mm
Number of layers	380
Length of the active part	$19.6X_0$
Number of WLS fibers per cell	18(bent at the front)
Thickness of the TYVEK	0.175±0.025mm

the side faces of the scintillator tiles are covered with white reflector paint.

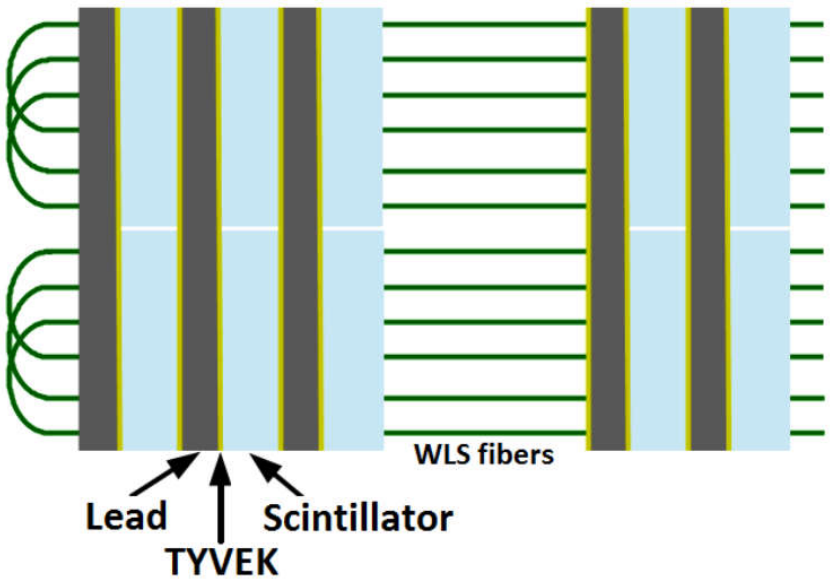

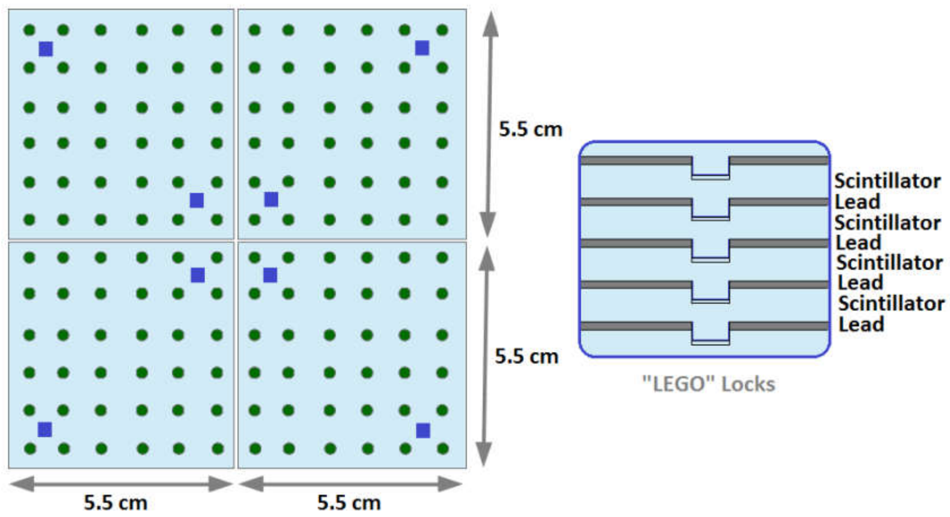

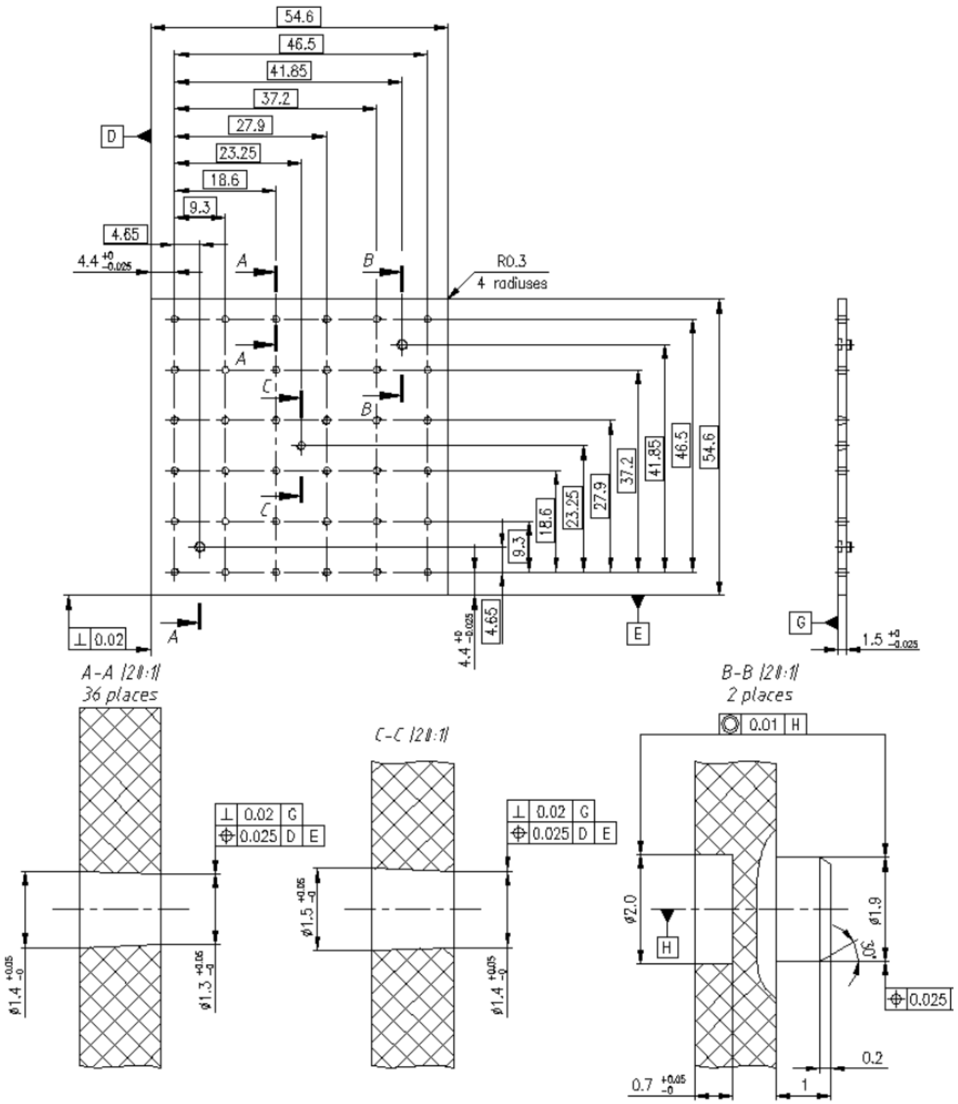

Figure 4.10: Technical drawing of the scintillator tiles of the FSC cell.

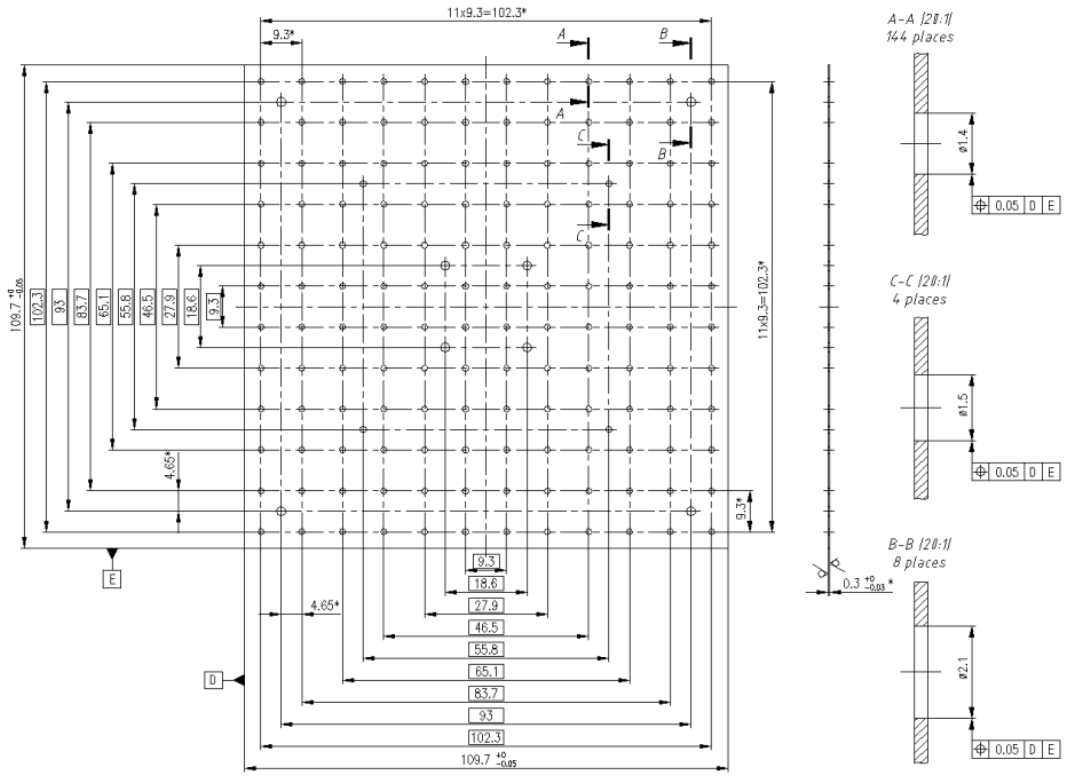

Figure 4.11: Technical drawing of the lead plates of the FSC module.

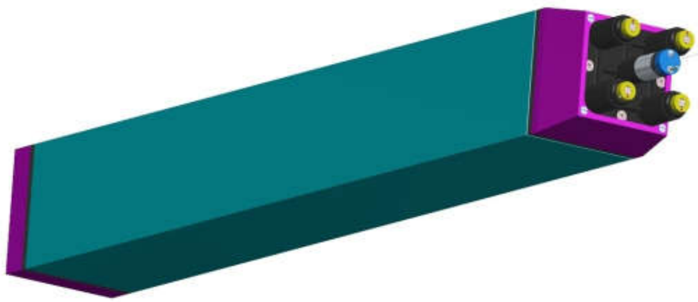

Figure 4.6: A global view of the assembled FSC module without PMT compartment.

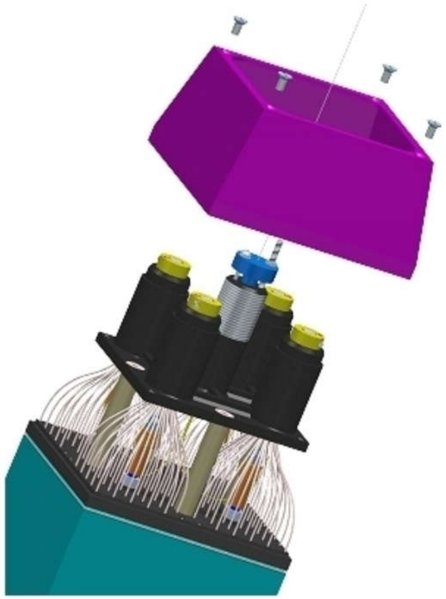

Figure 4.7: A back-side exploded view of the FSC module.

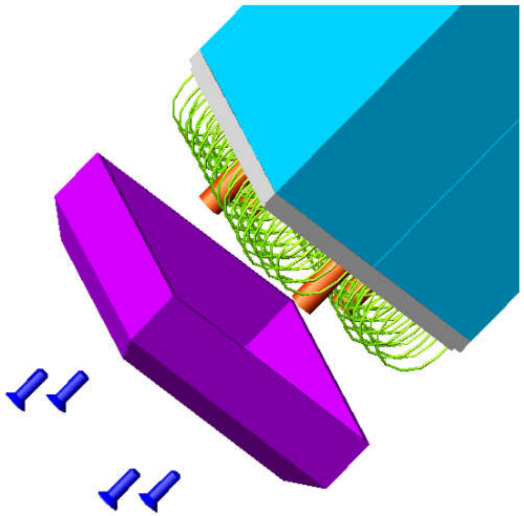

Figure 4.8: A front-side view of the FSC module showing the front cover, the WLS fibre loops, and the pressure plate.

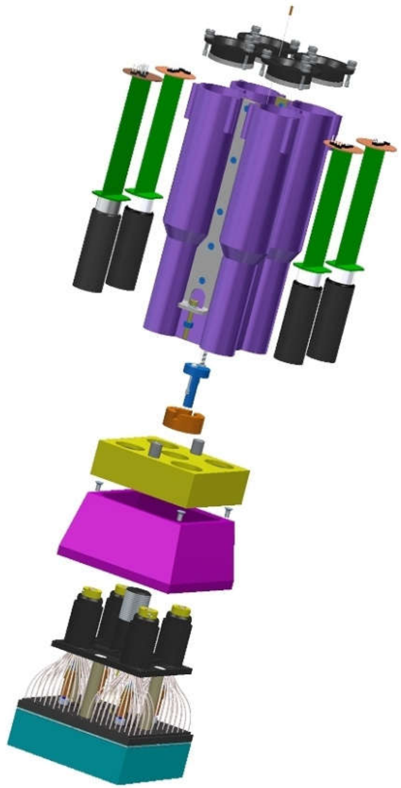

Figure 4.9: Exploded view of a fully assembled module.

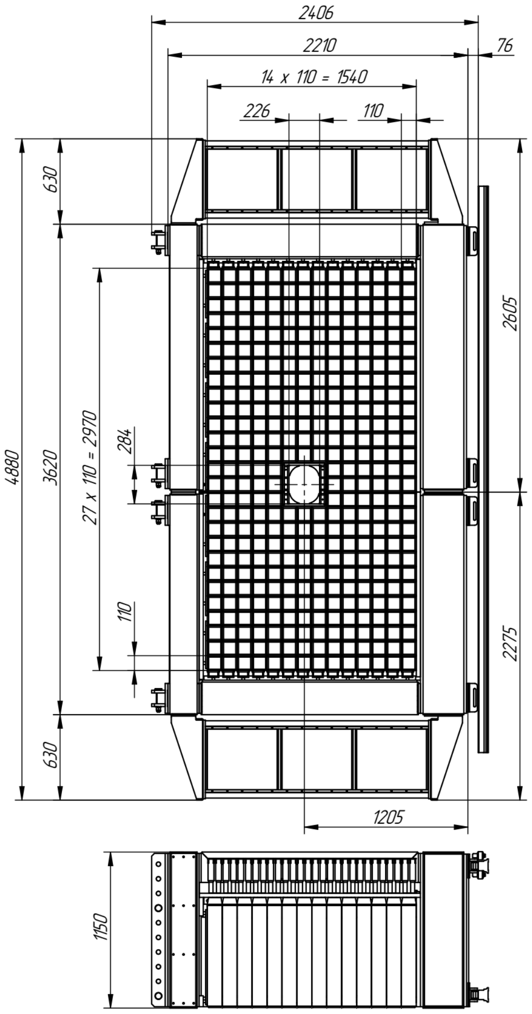

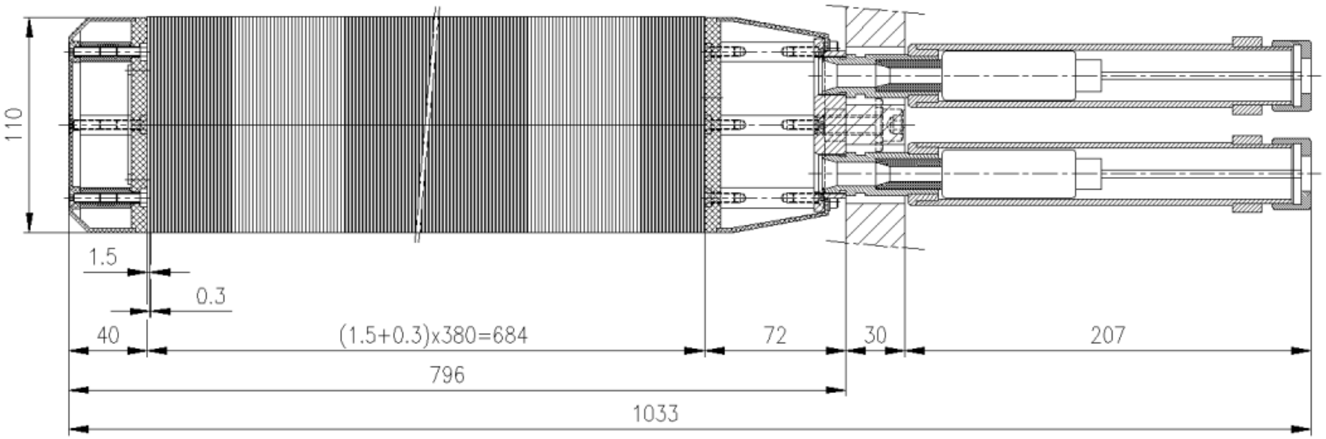

Figure 4.4: The global dimensions of a shashlyk FSC module of Type-2.

Figure 4.3: Dimensions of the closed FSC frame in the beam position.

28*54 cells FSCwall with One cell one module in the current PandaRoot

TGeoShape* ModuleShape = new TGeoBBox(name,cellxsize/2.,cellysize/2.,thickness/2.);

name = "FscModuleVolume"; TString medium = "carbon";

TGeoShape* TyvekShape = new TGeoBBox(name,cellxsize/2. - paperbundle,cellysize/2. - paperbundle,thickness/2. - paperbundle);

name = "FscTyvekVolume"; medium = "tyvek";

//Building and placing holder (for Scint+Lead layer) volumes inside tyvek volume

TGeoShape* LayerHolderShape = new TGeoBBox(name, cellxsize/2. - crystalspace, cellysize/2. - crystalspace, cell_thickness/2.);

name = "FscLayerHolderVolume"; medium = "Air";

//Building and placing Lead + Scint layer inside holder Volume

TGeoShape* LeadShape = new TGeoBBox(name, cellxsize/2. - crystalspace, cellysize/2. - crystalspace, Pb_thickness/2.);

name = "FscLeadVolume"; medium = "lead";

TGeoShape* SciShape = new TGeoBBox(name, cellxsize/2. - crystalspace, cellysize/2. - crystalspace, Sci_thickness/2.);

name = "FscSciVolume"; medium = "FscScint";

placing Lead + Scint 380 layers

//Building and placing Fibers inside FscModule Volume

TGeoShape* FiberHoleShape = new TGeoTube(name, 0., fiber_hole_r, (holder_thickness)/2.);

name = "FscFibHoleVolume"; medium = "air"; placing 6*6 matrix air holes

//FIbers itself inside holes

TGeoShape* FiberShape = new TGeoTube(name, 0., fiber_r, (holder_thickness)/2.);

name = "FscFiberVolume"; medium = "FscFiber";

Finally // placing Modules of Carbon inside top FSC (28*54 matrix cells FCSwall)

FSC Calibration

The calibration procedures: three levels with increasing precision

1. Pre-calibration (with vertical cosmic muon or minimum-ionising particle signals)
   - not precise enough and can not be used for the final FSC data analysis
   - But extremely useful at the detector initial setup and commissioning
2. Online –calibration
   - more precise and use physical events
   - The main goal is to give a correct energy response from the FSC during online data analysis, and draw operators' attention if the detector performance deteriorates for some reasons.
3. Offline –calibration
   - - Using constraints on the π^0 and η masses.
   - - Using the E/p ratio for electrons from decays.

Simulation results in RE-TDR -2015-002

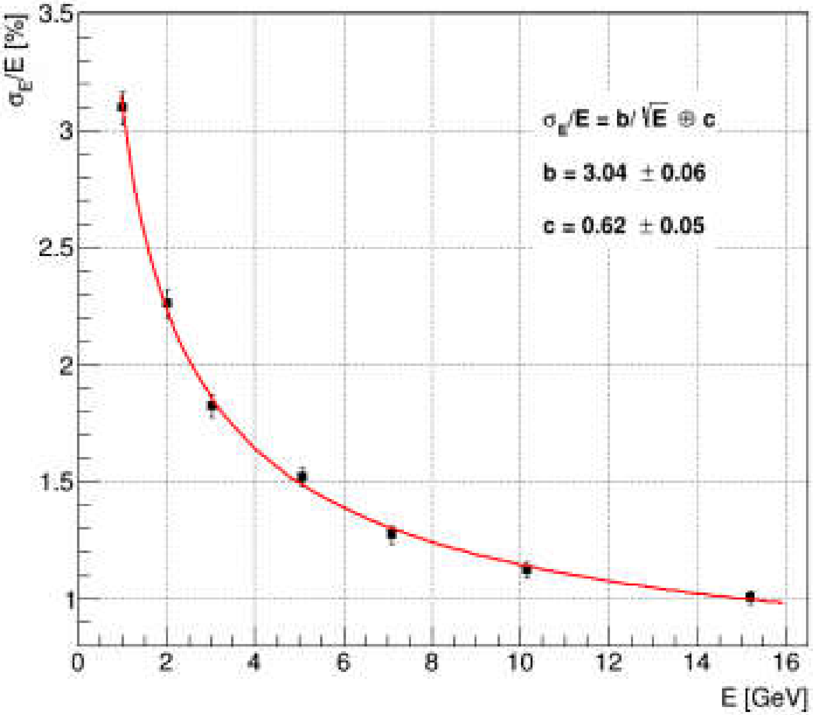

Figure 7.2: Simulated energy resolution as a function of the incident electron energy between 1 GeV and 15 GeV for a digitised signal from the FSC.

$$\frac{\sigma_E}{E} = \frac{b}{\sqrt{E/\mathrm{GeV}}} \oplus c.$$

with Type-2 modules yield $b = (3.15 \pm 0.43)\,\%$, $c = (1.37 \pm 0.11)\,\%$ (see Sec. 8.2.1). The discrepancy in the constant term may be caused by uncertainties in the calibration coefficients of test-beam data. Nevertheless, we can conclude that the digitisation procedure is accurately described in our simulation.

The conclusion: The digitization procedure is accurately described in our simulation.

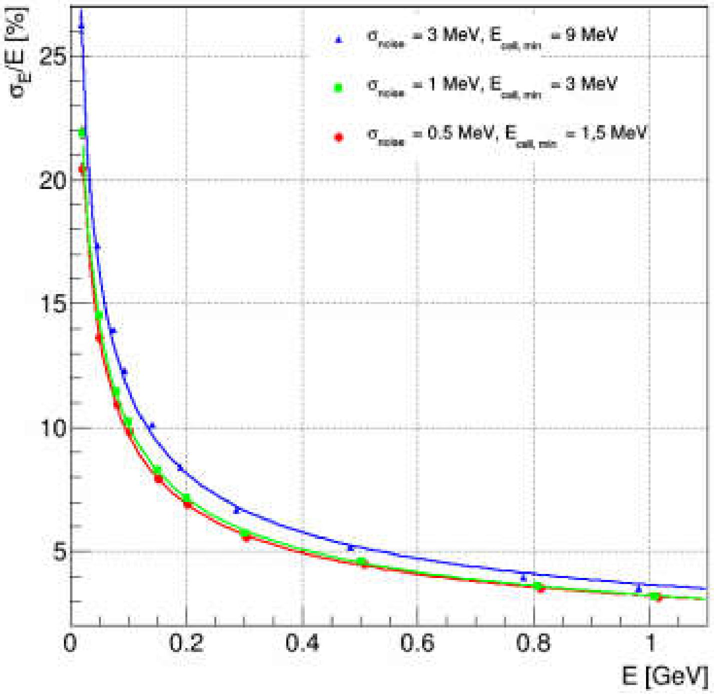

Figure 7.3: Comparison of the energy resolutions for three different single-cell reconstruction thresholds. The

The study of Single-cell reconstruction thresholds.

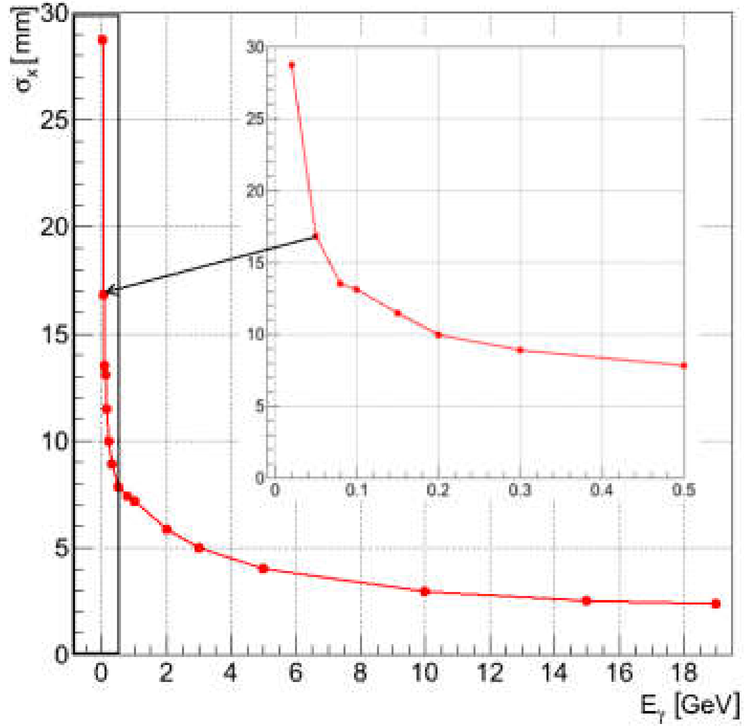

Figure 7.4: Position resolution in x-direction for photons from 20 MeV to 19 GeV.

of ~ 28 mm (half of the cell size). The point at 19 GeV energy is also simulated in order to compare with test-beam data. As mentioned in Sec. 8.2.1, the experimental resolution at 19 GeV at the centre of the cell is 3 mm, while our simulation with PandaRoot gives 2.4 mm. Thus the agreement is reasonable.

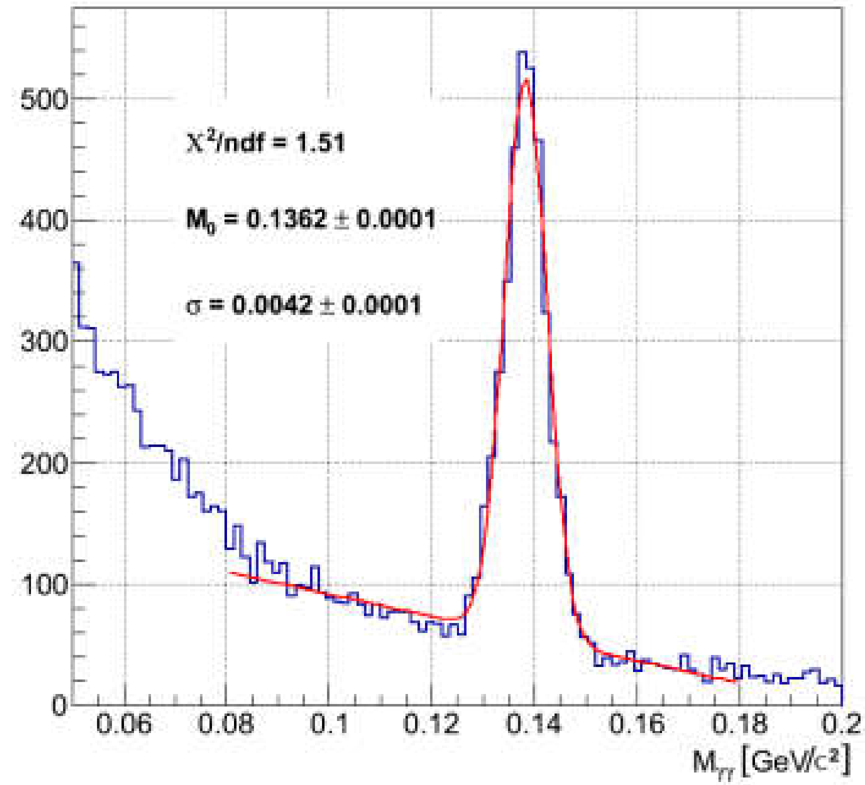

Figure 7.5: Invariant-mass spectrum of photon pairs from decays of π^0 with energy up to 15 GeV in the FSC acceptance.

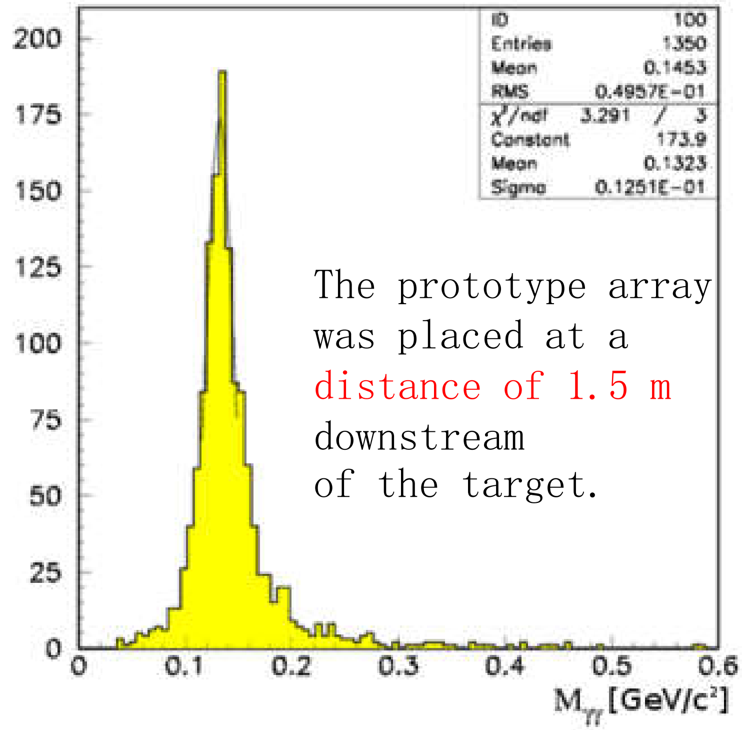

Figure 8.16: Spectrum of the reconstructed invariant mass of π^0 mesons between 1 and 2 GeV energy. The distance between the test-beam target and the FSC prototype was 1.5 m.

Considering the experimental energy and position resolutions, the contribution of the position resolution will be significantly smaller due to the large distance of ~7 m of the FSC to the target in the final setup at $\overline{\text{P}}$ANDA. One may expect an invariant-mass resolution in the order of 4 MeV/c^2 for 1-2 GeV π^0

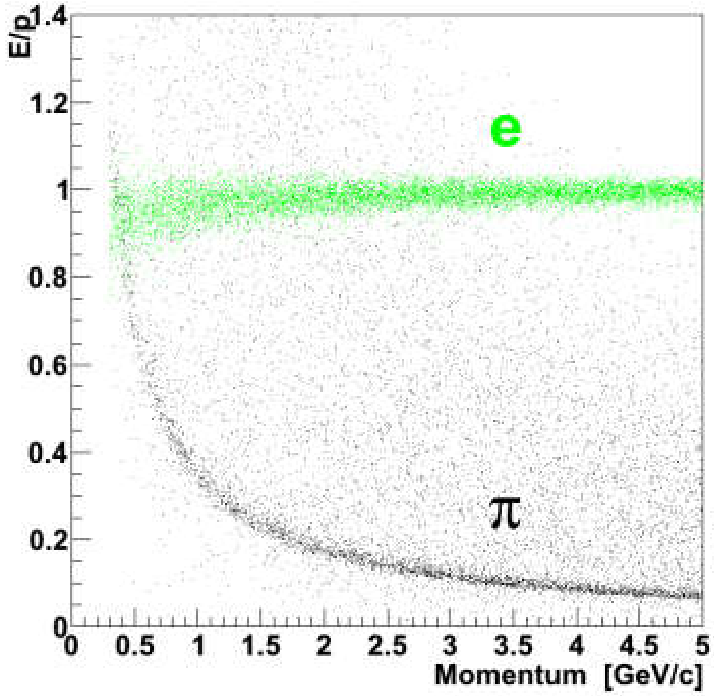

Figure 7.8: Simulated E/p ratio as function of the track momentum for electrons (green) and pions (black) in the momentum range between 0.3 GeV/c and 5 GeV/c.

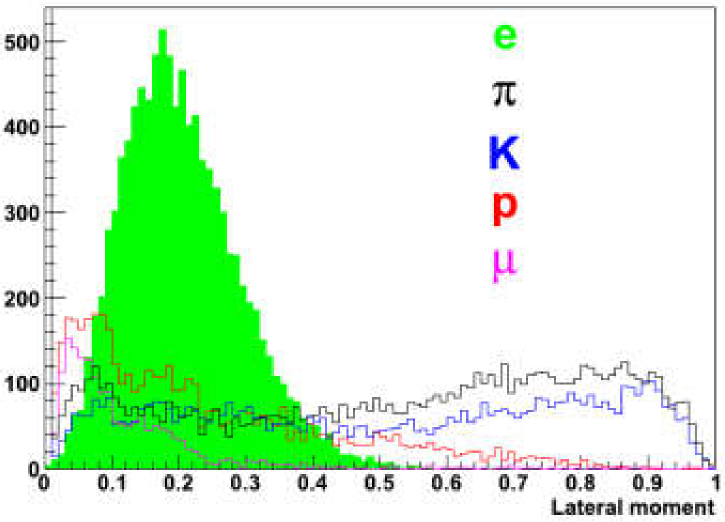

Figure 7.9: The lateral moment of the FSC cluster for electrons, muons and hadrons.

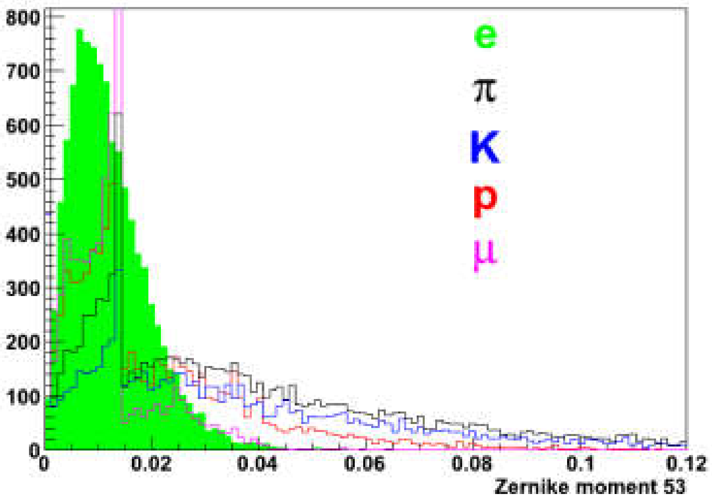

Figure 7.10: Zernike moment z_{53} for electrons, muons and hadrons.

Electron Identification

To demonstrate the advantages of the MLP network, we show here a result obtained for the barrel part of the $\overline{\mathrm{P}}$ANDA Target Spectrometer EMC. The training of the MLP was achieved with a data set of 850.000 single tracks for each particle species (e, μ, π, K and p) in the momentum range between 200 MeV/c and 10 GeV/c in such a way that the output values are constrained to be 1 for electrons and -1 for all other particle types. In total, 10 input variables have been used, namely E/p, the momentum p, the polar angle θ of the cluster, and 7 shower-shape parameters (E_1/E_9, E_9/E_{25}, the lateral moment of the shower, and 4 Zernike moments).

The response of the trained network to a set of test data of single particles in the momentum range between 300 MeV/c and 5 GeV/c is shown in Fig. 7.11. The logarithmically scaled histogram shows that an almost clean electron recognition with a small contamination of muons ($< 10^{-5}$) and hadrons (0.2% for pions, 0.1% for kaons and $< 10^{-4}$ for protons) can be obtained by applying a cut on the network output. The plan is to incorporate such a method in the reconstruction algorithm.

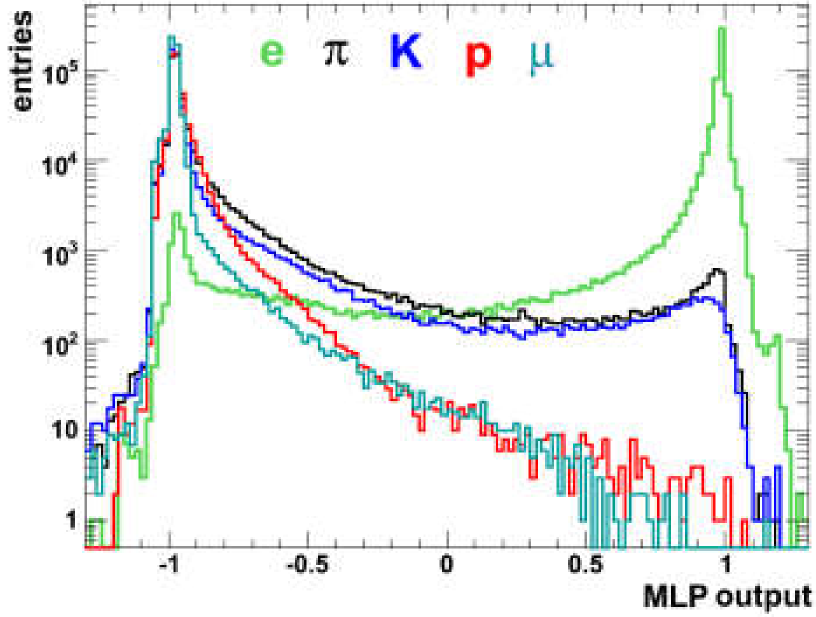

Figure 7.11: Simulation of MLP output for electrons and other particle species in the momentum range between 300 MeV/c and 5 GeV/c for the barrel part of the Target Spectrometer EMC.

What do we need to do ?

- Update of FSC geometry
- Further Study by simulation data
  - the offline-calibration by π^0events or electron E/p
  - Reconstruction of photon and electron, and the energy and spatial resolutions, and π^0reconstruction
  - Electron identification (To find the PID code)
  - etc.

Some results of Type-2 test

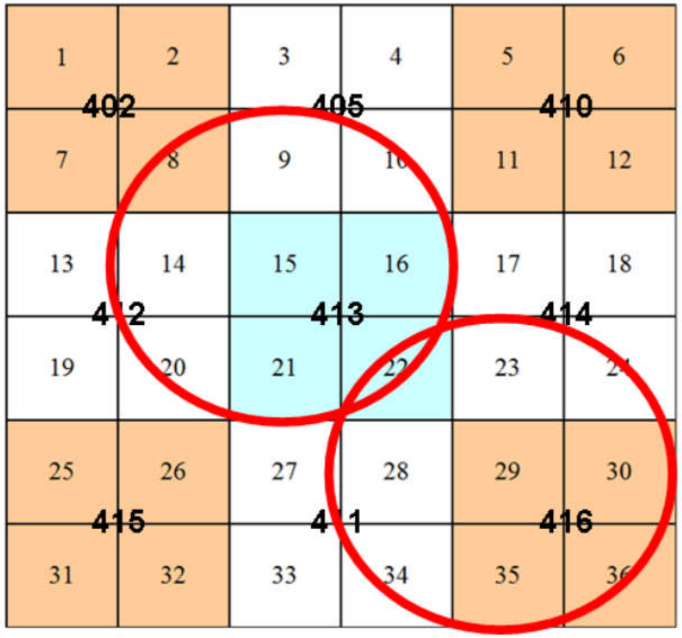

Figure 8.18: The labelling of the 6×6 detector cells of the test matrix of 3×3 detector modules at the tagged-photon facility at MAMI. Two main regions of impact are marked by red circles [5].

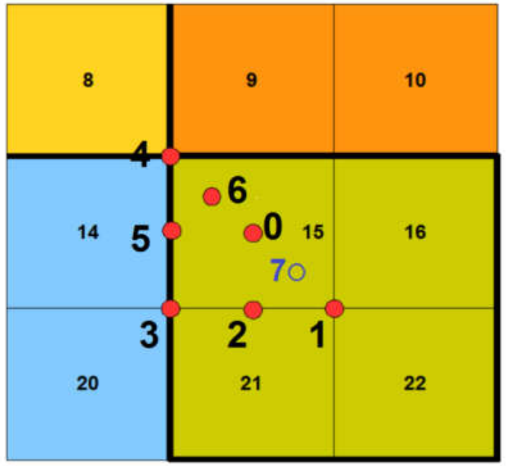

Figure 8.19: The chosen beam positions (red bullets) projected onto the front face of the test matrix [5].

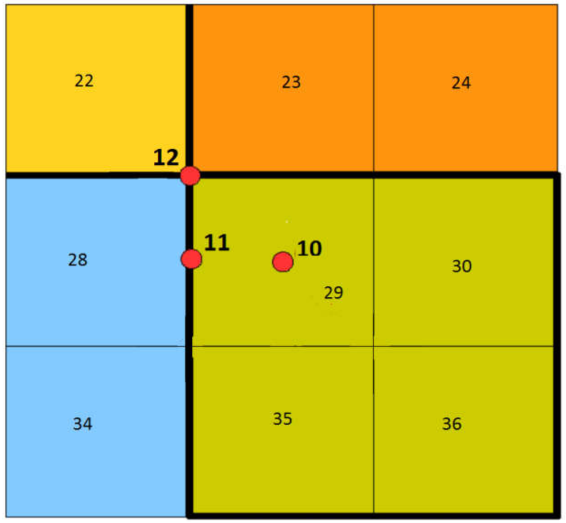

Figure 8.20: The chosen beam positions (red bullets) projected onto the front face of the test matrix [5].

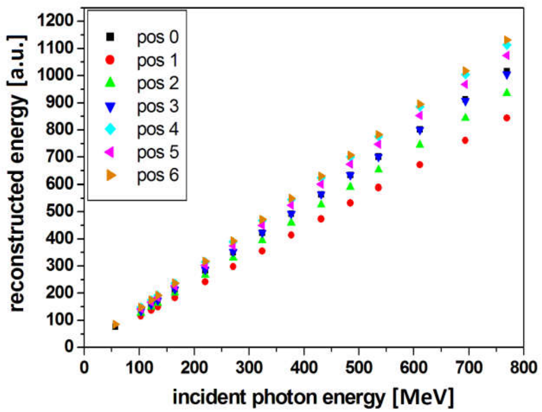

Figure 8.22: Linearity of the deduced energy response over the entire range of photon energies measured for different points of impact [5].

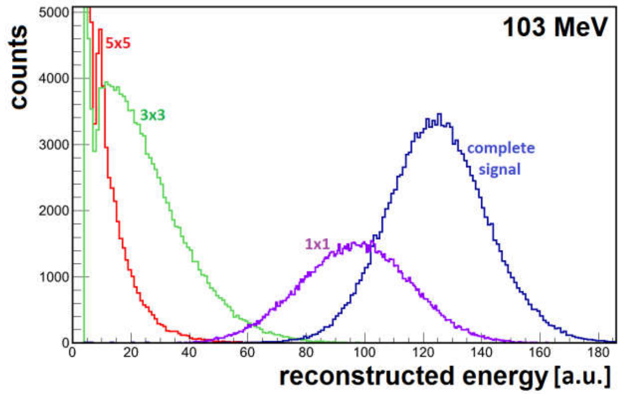

Figure 8.23: Energy response of the Type-2 prototype for 103 MeV photons. The different spectra are explained in the text [5].

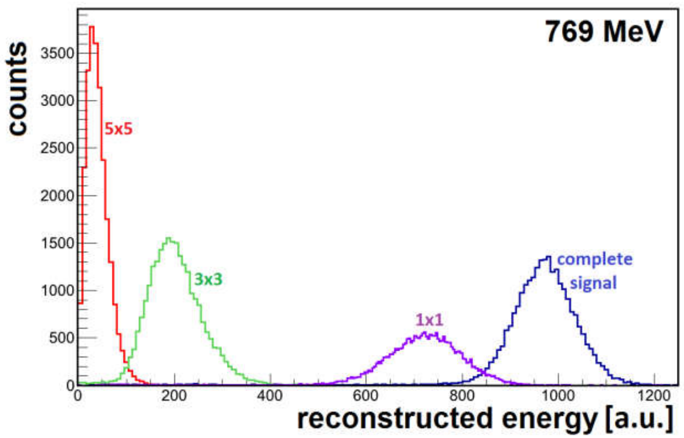

Figure 8.24: Energy response of the Type-2 prototype for 769 MeV photons. The different spectra are explained in the text [5].

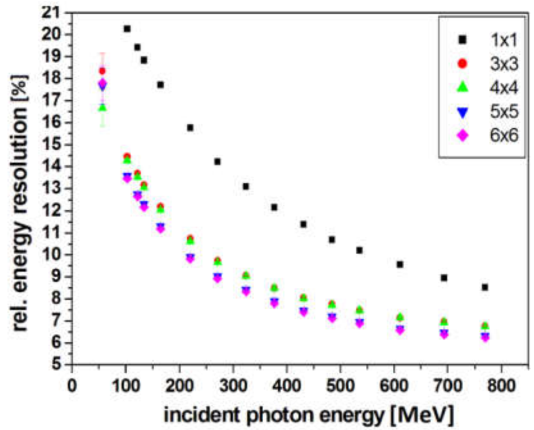

Figure 8.25: Relative energy resolution of the Type-2 prototype obtained by summing the energy deposition in different cluster sizes [5].

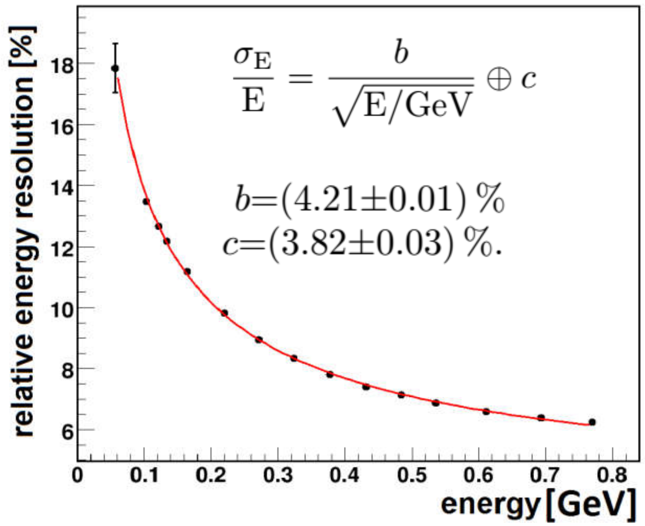

Figure 8.26: Relative energy resolution of the whole matrix of the Type-2 detector composed of 6×6 cells [5].

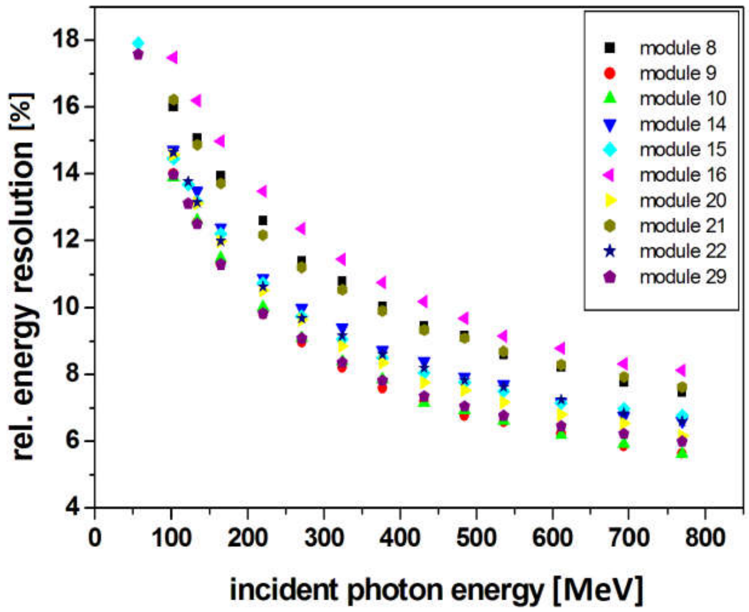

Figure 8.27: Relative energy resolution as function of the photon energy in the entire energy range when photons hit the centre of different cells as the central cell of a 3×3 matrix of the Type-2 detector [5].

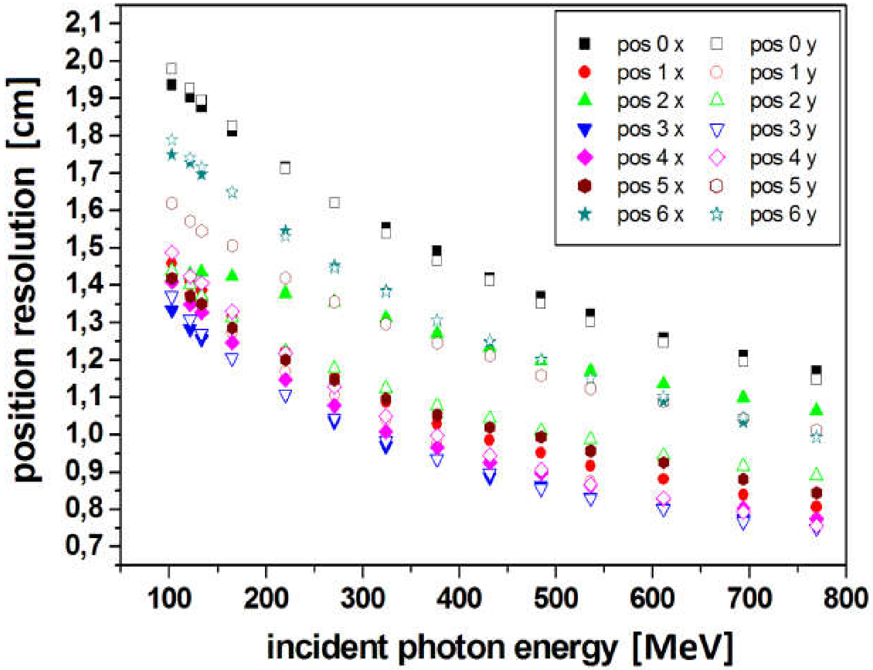

Figure 8.28: Achieved position resolutions as a function of photon energy for different beam positions as marked in Fig. 8.19 [5].

Time resolution of a single cell

The timing performance will be a relevant parameter in reconstructing the individual events in a trigger-less data acquisition (see Chap. 5), as envisaged for $\overline{\mathrm{P}}$ANDA. A first estimate has been obtained by measuring the relative timing between two adjacent detector cells, since both obtain a very similar energy deposition if the beam hits in the middle between two cells. This measurement at different photon energies allows to deduce the absolute time resolution as a function of energy deposition in a wide energy range. Figure 8.29 shows a typical timing spectrum taken at an energy deposition of 290 MeV in one of the two considered cells. Figure 8.30 shows the deduced timing resolution as a function of deposited energy. A value of 100 ps can be expected at an energy deposition of 1 GeV.

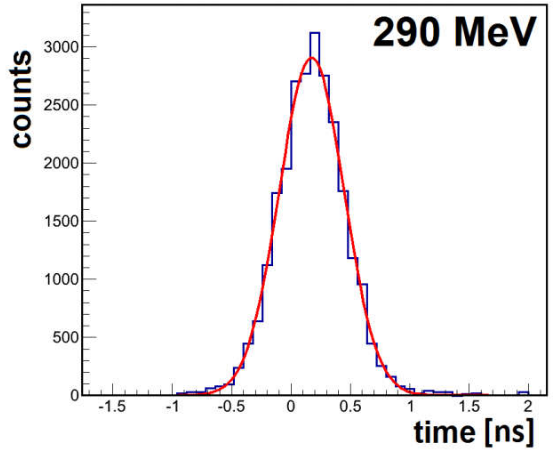

Figure 8.29: Coincidence timing between two adjacent cells at a typical energy deposition of 290 MeV in both cells. The resolution is deduced by a fit with a Gaussian shape [5].

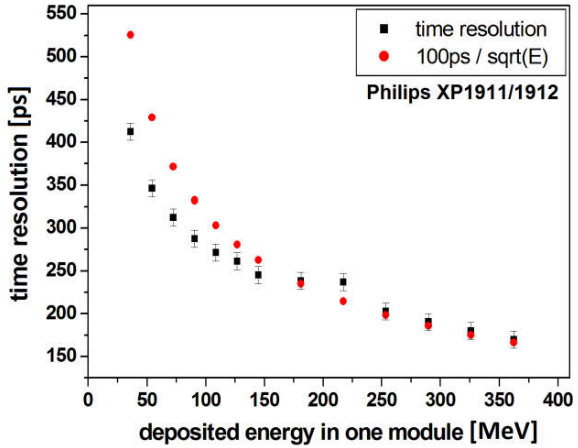

Figure 8.30: Achieved time resolution of a single cell as a function of deposited shower energy. The red dots correspond to a resolution of 100 ps/$\sqrt{\mathrm{E/GeV}}$ with E given in units of GeV [5].

Type-2

The end

The Type-1 module had a cell size of 11×11 cm^2.

The Type-2 and Type-3 modules have a cell size of 5.5×5.5 cm^2 and one module consists of 4 cells. For all three prototypes, lead plates of 11×11 cm^2 size are used for either one cell (Type-1) or for four cells (Type-2 and Type-3). For the Type-2 and Type-3 modules, scintillator plates with a size of 5.5×5.5 cm^2 are used. Type-2 scintillator tiles were produced by cutting Type-1 scintillator tiles into four quadratic parts and thus have only one alignment pin at the outer corner. There was no reflective material between tiles and the lead plates. Type-3 scintillator tiles were moulded and have all four alignment pins. Besides, for the Type-3 Tyvek sheets are placed as a reflector material between the scintillator plates and the lead plates.

Introduction

The physics program of the PANDA project at the international FAIR facility at GSI (Germany) is based on a state-of-the-art universal detector for strong interaction studies at high intensity cooled antiproton beam with an energy up to 15 GeV.

This program relies heavily on the capability to measure photons with excellent energy and position resolution. For this purpose PANDA has proposed to employ electromagnetic calorimeters using two different technologies: a compact calorimeter around the target based on lead tungstate crystals and a fine-segmented Shashlyk-type calorimeter in the forward region (Figure 1).

PANDA physics program requires 4π angular coverage of photon detection, which is achieved mainly by the target spectrometer EMC.

However, to measure everything in the forward region with angles less than 5° in vertical plane and 10° in horizontal plane, forward spectrometer EMC is used.

The target spectrometer EMC is going to be built from the lead tungstate scintillating crystals (PWO).

It has been already realized in the CMS, ALICE and PRIMEX electromagnetic calorimeters.

Table 3.1: Requirements for the $\overline{\mathrm{P}}$ANDA FSC. Rates and doses are based on a luminosity of $L = 2{\cdot}10^{32}$ $cm^{-1}s^{-1}$.

Common properties	Required performance value
energy resolution σ_E/E	$\approx$ (2-3)% $/\sqrt{E/GeV}$ $\oplus$ 1%
energy threshold (photons) E_{thres}	10 MeV (20 MeV tolerable)
energy threshold (single cell) E_1	3 MeV
noise (energy equiv.) σ_{Enoise}	1 MeV
angular coverage	0°- 5°
energy range from E_{thres} to	15 GeV
spatial resolution	3.5 mm
load per cell	$\approx$ 1 MHz
radiation hardness (maximum integrated dose)	10 kGy

Table 3.1: Requirements for the $\overline{\mathrm{P}}$ANDA FSC. Rates and doses are based on a luminosity of $L = 2{\cdot}10^{32}$ $cm^{-1}s^{-1}$.

Common properties	Required performance value
energy resolution σ_E/E	$\approx$ (2-3)% $/\sqrt{E/GeV}$ $\oplus$ 1%
energy threshold (photons) E_{thres}	10 MeV (20 MeV tolerable)
energy threshold (single cell) E_1	3 MeV
noise (energy equiv.) σ_{Enoise}	1 MeV
angular coverage	0°- 5°
energy range from E_{thres} to	15 GeV
spatial resolution	3.5 mm
load per cell	$\approx$ 1 MHz
radiation hardness (maximum integrated dose)	10 kGy

Title	Value	Units
Overall detector width (x direction)	4.9	m
Overall detector height (y direction)	2.2	m
Overall detector depth (z direction)	1150	mm
Overall detector weight (see Table 4.4)	14.7	tons
Number of channels (including beam pipe zone)	1512	pcs
Number of modules (including beam pipe zone)	378	pcs
Module weight	21	kg
Module cross section	110×110	mm^2
Cell cross section	55×55	mm^2
Scintillator tile thickness	1.5	mm
Lead plate thickness	0.275	mm
Beam pipe zone	$9 = (3\times3)$	modules

Table 4.1: Main mechanical properties of the FSC.

FSC components, geometry and dimensions

The FSC is located behind the dipole magnet of the $\overline{\text{P}}$ANDA Forward Spectrometer, just downstream of the RICH detector, and is designed in planar geometry, covering the most forward angular range up to 5° in the vertical and 10° in the horizontal direction. The exact position and the dimensions of the FSC are defined by the size of the central hole in the forward endcap EMC of the Target Spectrometer [1]. The active volume of the FSC consists of 54×28 cells. The overall dimensions of the detector frame are 3.6 m in width and 2.2 m in height.

Important parts of the mechanical design of the module are the LEGO-type locks for the scintillator tiles. Four pins per tile fix the relative position of the scintillators and provide 0.3 mm gaps which are sufficiently wide to place the 0.275 mm thick lead plates without optical contact between lead and scintillator (Fig. 4.5). The module is wrapped with reflective material. Internal edges of the tiles are covered by white paint to provide optical isolation and to increase the light output.

1.2.7 Calibration and Monitoring

The FSC should have about 3 % energy resolution (stochastic term) and 3.5 mm position resolution (at the centre of the cell). To fully utilise such a good performance one needs to have a monitoring system to measure variations of the PMT gain at the percent level or better in order to compensate the gain changes.

Each FSC cell needs to be periodically calibrated. A pre-calibration with vertical cosmic-ray muons is a fast and reliable method to adjust the PMT gains, especially for the initial settings.

The fine calibration of the FSC exploiting neutral pion decays, will apply algorithms which are well known in high-energy physics. The second algorithm exploits the E/p (energy/momentum) ratio for electrons from decays of miscellaneous particles. In this method we transfer the energy scale from the forward tracker to the FSC by measuring the E/p ratio for isolated electrons (E from the calorimeter, p from the tracker). The fine calibration by these two methods can be simultaneously performed for the entire FSC within a couple days.

Simulation
Reconstruction
Digitisation procedures
Simulations focused on the threshold dependence of energy and spatial resolution for reconstructed photons and electrons, the influence of the material budget in front of the FSC, and the electron-hadron separation. Because most of the physics channels have very low production cross section, typically between pb and nb, a background rejection power up to 10^9 has to be achieved. This requires an electromagnetic calorimeter which allows an accurate photon reconstruction in the energy range from 10-20MeV to 15 GeV and an effective and clean electron hadron separation.

4.2.5 The photo sensor

The $\overline{\text{P}}$ANDA Forward Spectrometer Calorimeter has to register energy depositions in a high dynamic range with low noise at a high rate of forward-emitted photons. Taking into account the position of the calorimeter outside of the magnetic field, the most appropriate photo detector which can cope with the expected environment is a photomultiplier tube (PMT). In this section we will describe the se-

Table 1.6 gives an overview over the most important design parameters of the shashlyk modules for version A and B.

property	version A	version B
lateral dimension of a module	$(11 \times 11)\ cm^2$ ($\approx 0.8°$)	$(11 \times 11)\ cm^2$ ($\approx 0.8°$)
lateral dimension of a single cell	$(5.5 \times 5.5)\ cm^2$ ($\approx 0.4°$)	$(5.5 \times 5.5)\ cm^2$ ($\approx 0.4°$)
length of the active part	19.6 X_0 (69.8 cm)	19.6 X_0 ($\approx$ 81 cm)
total module length (without PMT)	79.3 cm	90.5 cm
thickness of the lead plates	0.275 mm	0.275 mm
thickness of the scintillator tile	1.5 mm	1.5 mm
thickness of the TYVEK (760 pc.)	-	$(0.175 \pm 0.025)\ mm$
air gap scintillator-lead/TYVEK	37.5 μm	12.5 μm
number of WLS fibers per cell	18 (bent at the front)	18 (bent at the front)
length of one bent WLS fiber	$\approx$ 1.9 m	$\approx$ 2.1 m
type and diameter of a WLS fiber	Bycron (BCF-91A), 1.0 mm	Kuraray (Y-11(200)), 1.0 mm
mass of one module	$\approx$ 22.5 kg	$\approx$ 22.9 kg

Table 1.6: Design values of the shashlyk EMC modules. The values are taken from [TDf15, KSM09].

property	shashlyk EMC	target EMC
number of individual units	$378 \times 4 = 1512$	15552
number of readout channels	1512	< 31104
effective density $[g/cm^3]$	2.7^A / 2.62^B	8.28
effective radiation length X_0 [cm]	3.49^A / 4.05^B	0.89
effective Molière-Radius R_M [cm]	5.98	2.0
active calorimeter depth	19.6 X_0	22.5 X_0
relative unit size	0.92 R_M	$\approx$ 1.07 R_M

Table 1.8: Parameters of the shashlyk EMC for calorimeter physics in comparison to the target EMC made of PWO crystals [TDf15, KSM09, TDe09]. The super-scripts ^{A} and ^{B} indicate the version of the modules. The number of readout channels of the target EMC is smaller than the given value, since crystals of the forward end cap which are read out by a VPTT have only one channel per unit.

The comparison shows that, due to the use of a low Z organic scintillator material, the effective radiation length and the Molière-Radius are significantly larger for the shashlyk EMC. Therefore, the individual detector units have to be larger in all dimensions.

parameter	value
diameter of the entrance window	25 mm
number of dynodes	10
cathode material	bi-alkali
spectral response	300 nm - 650 nm
wavelength of max. quantum efficiency λ_{max}	420 nm
quantum efficiency at λ_{max}	27 %
quantum efficiency at 500 nm	14 %
gain at 1500 V	$2 \cdot 10^6$
output signal rise time	1.6 ns
electron transit time	16 ns
variation of transit time	0.7 ns
pulse height linearity @ 1500 V ($\pm$ 2%)	100 mA

Table 1.7: Properties of the Hamamatsu R7899 PMTs, which are currently favored for the readout of the shashlyk modules [Ham00].

One module consists of 380 layers of 0.275 mm thick lead sheets and 1.5 mm thick scintillator tiles [TDf15]. In comparison to the KOPIO modules, the number of layers has been increased by 26.6 % from 300 to 380 which was necessary to provide a sufficient energy resolution for high energies up to 15 GeV. Since the results obtained with the KOPIO modules concerning the energy resolution at low energies were already sufficient and since a further decrease of the lead sheet size would increase the module length even more, it was decided to adapt the concept. To reach the envisaged position resolution and to increase the count rate capability each $(11 \times 11)\ cm^2$ large module is divided into four cells with a front face of $(5.5 \times 5.5)\ cm^2$ each which is a little bit smaller than the effective Molière-Radius of 5.98 cm [TDf15]. While the lead sheets are common for all four cells, the scintillator tiles are separated for the four cells and optically isolated with white paint. For the scintillator tiles, an organic plastic scintillator material is used. Based on earlier experiences with the KOPIO modules concerning the radiation hardness and the light output it was decided to use polystyrene doped with 1.5 % paraterphenile and 0.04 % 1,4-Bis-(5-phenyloxazol-2-yl)-benzol (POPOP) [TDf15]. The tiles are produced by injecting the melted raw material into a specially manufactured mould. To fix the position of the layers relative to each other, pin-holes, also called "LEGO" locks, are added to the scintillator tiles which are shown in the right part of figure 1.40. Each cell is intersected by 36 holes with a diameter if 1.3 mm, which are arranged as a 6×6 matrix with a distance between two holes of 9.3 mm [TDf15]. Through this holes 18 1.0 mm thick wavelength shifting (WLS) fibers are inserted, bend at the front of the module and reinserted in another hole. The 36 ends of these fibers, which collect the light from the scintillator tiles are bundled at the rear side of the module and read out with a PMT. To stabilize the module mechanically four thin metal bars (one per cell) are inserted through longitudinal holes in the module. Figure 1.41 shows a 3D drawing of the shashlyk module with its four cells and a detailed view of its front and rear part with open covers.